

INFLUENCE OF RELATIVISTIC EFFECTS ON ELECTRON-LOSS CROSS SECTIONS OF HEAVY AND SUPERHEAVY IONS COLLIDING WITH NEUTRAL ATOMS

I. Yu. Tolstikhina^{a,b}, *I. I. Tupitsyn*^c, *S. N. Andreev*^a, *V. P. Shevelko*^{a*}

^a *Lebedev Physical Institute, Russian Academy of Sciences
119991, Moscow, Russia*

^b *Moscow Institute of Physics and Technology
141700, Dolgoprudny, Moscow Region, Russia*

^c *Department of Physics, St. Petersburg State University
198504, Saint-Petersburg, Russia*

Received January 10, 2014

The influence of relativistic effects, such as relativistic interaction and relativistic wave functions, on the electron-loss cross sections of heavy and superheavy atoms and ions (atomic number $Z \gtrsim 92$) colliding with neutral atoms is investigated using a newly created RICODE-M computer program. It is found that the use of relativistic wave functions changes the electron-loss cross section values by about 20–30 % around the cross-section maximum compared to those calculated with nonrelativistic wave functions. At relativistic energies $E \geq 200$ MeV/u, the relativistic interaction between colliding particles leads to a quasiconstant behavior of the loss cross sections $\sigma_{EL}^{rel} \sim \text{const}$, to be compared with the Born asymptotic law $\sigma_{EL}^B \sim \ln E/E$.

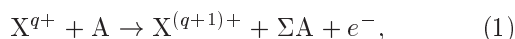
DOI: 10.7868/S0044451014070013

1. INTRODUCTION

The relativistic effects, i. e., relativistic wave functions and relativistic interaction, already become important in atoms and ions with the nuclear charges $Z \gtrsim 30$ (see, e. g., [1–4]) and are taken into account in calculation of the radiative atomic characteristics such as binding energies, oscillator strengths, transition probabilities, etc.

As concerns the collision properties, the influence of relativistic effects on excitation, radiative recombination, and electron-capture and electron-loss cross sections for heavy ions colliding with neutral atoms are discussed in various review articles and books [5–11].

Here, we investigate the influence of relativistic effects on the electron-loss cross sections of heavy and superheavy ($Z \geq 92$) many-electron ions colliding with neutral atoms, i. e., for the reactions



where X^{q+} denotes the incident projectile ion with the charge q and A is the target atom; ΣA indicates that the outgoing target atom A can be excited or ionized.

Together with another charge-changing process — electron capture — electron loss plays a key role in many fields of atomic, accelerator, and plasma physics: in production of long-lived ion beams in accelerators and requirements for vacuum conditions [12], ion thermonuclear fusion program [13], particle tumor therapy [14], heavy-ion probe beam (HIPB) diagnostics [15], etc.

Another problem showing the importance of charge-changing processes is closely related to nuclear physics. Recently, a detection of superheavy elements with atomic numbers up to $Z = 118$ in nuclear fusion evaporation reactions became possible using the gas-filled separators based on charge-state equilibrium phenomena (see, e. g., [16, 17]). Properly setting the magnetic rigidity of the separators requires an accurate knowledge of ion velocity-to-charge ratio v/\bar{q} , where \bar{q} is the average (equilibrium) ion charge after the separator. In the atomic approach, the average charge and equilibrium charge-state fractions can be expressed in terms

*E-mail: shev@sci.lebedev.ru

of the electron-loss and capture cross sections [18] calculations of which in the case of superheavy elements require accounting for the relativistic effects.

In our previous papers devoted to the calculation of electron-loss cross sections (see, e. g., [19, 20]), we used the RICODE computer program, which employs the relativistic interaction between colliding particles but nonrelativistic radial wave functions for the bound and continuum states of the projectile active electron. This code provides a reasonable agreement with experimental electron-loss cross sections for heavy many-electron positive ions (up to uranium ions) colliding with neutral atoms at ion energies $1 \text{ MeV/u} < E < 100 \text{ GeV/u}$. In the case of few-electron heavy projectiles (H- and He-like ions), it was found that the influence of relativistic effects on the wave functions is strong and leads to a severalfold reduction of the electron-loss cross sections (see, e. g., [21, 22]).

The aim of this paper is to investigate the influence of the relativistic effects on the electron-loss cross sections for heavy and superheavy many-electron ions colliding with neutrals using a newly created RICODE-M program. It is found that in the vicinity of the cross-section maximum, the influence of the relativistic effects on the wave functions is large for neutral and low-charged atoms and ions, and at relativistic energies $E > 200 \text{ MeV/u}$, the influence of the relativistic ion-atom interaction plays a major role and significantly changes the cross section dependence on the collision energy compared with the Born asymptotic behavior. A description of the RICODE-M program is also given.

2. THE RICODE-M COMPUTER PROGRAM

The RICODE-M program (Relativistic Ionization CODE Modified) is created to calculate single-electron loss cross sections for reaction (1) and is based on the relativistic Born approximation [23]. The general structure of RICODE-M is similar to that of the previous RICODE program [19] but with one important difference: RICODE-M generates relativistic radial wave functions for both bound and continuous states of the projectile active electron, while RICODE applies nonrelativistic wave functions. In both codes, the relativistic (magnetic) interaction between colliding particles is used.

2.1. Core potentials, wave functions, and binding energies

In RICODE-M, the radial wave functions $P(r)$ of the active electron in the bound and continuum states

are calculated by numerically solving the Schrödinger-type equation with relativistic central-symmetric potential $U_c(r)$ of the atomic core and a given energy ε :

$$\left[-\frac{1}{2} \frac{d^2}{dr^2} + \frac{l(l+1)}{2r^2} + \frac{1}{\omega} U_c\left(\frac{r}{\omega}\right) \right] P(r) = \varepsilon P(r), \quad (2)$$

where the scaling factor ω is an eigenvalue of Eq. (2). The radial wave functions $P(r)$ of the projectile active electron in the bound and continuous states are normalized as

$$\int_0^\infty P_{nl}^2(r) dr = 1, \quad (3)$$

$$\int_0^\infty P_{\varepsilon\lambda}(r) P_{\varepsilon'\lambda}(r) dr = \pi\delta(\varepsilon - \varepsilon'),$$

where n and l denote the principal and orbital quantum numbers of the bound electron, and ε and λ are the energy and orbital quantum numbers of the ionized electron.

The core potential $U_c(r)$ in (2) is a relativistic local potential constructed based on the density functional theory (DFT) in the local density approximation (LDA). The potential $U_c(r)$ is created by the projectile nucleus and the rest electrons and consists of three parts:

$$U_c(r) = U_{nucl}(r) + U_{coul}(r) + U_{exc}(r). \quad (4)$$

The nuclear potential $U_{nucl}(r)$ is given by

$$U_{nucl}(r) = \int \frac{\rho_{nucl}(r')}{|\mathbf{r} - \mathbf{r}'|}, \quad (5)$$

where expression for the nuclear density $\rho_{nucl}(r)$ depends on the nuclear model to be used in RICODE-M (a point, volume, or Fermi models); $U_{coul}(r)$ and $U_{exc}(r)$ denote the Coulomb and exchange interaction potentials between core electrons.

For bound states, the binding energies $\varepsilon < 0$ are found from the subroutine HFDD of the RICODE-M program by solving the relativistic Dirac-Fock radial equations (see [24]):

$$\begin{aligned} c \left(-\frac{d}{dr} + \frac{\kappa}{r} \right) Q_{n\kappa}(r) + \left[U_{nucl}(r) + \frac{Y_{n\kappa}(r)}{r} \right] \times \\ \times P_{n\kappa}(r) = \varepsilon_{n\kappa} P_{n\kappa}(r) - \frac{X_{n\kappa}^Q(r)}{r}, \\ c \left(\frac{d}{dr} + \frac{\kappa}{r} \right) P_{n\kappa}(r) + \left[U_{nucl}(r) + \frac{Y_{n\kappa}(r)}{r} - 2c^2 \right] \times \\ \times Q_{n\kappa}(r) = \varepsilon_{n\kappa} Q_{n\kappa}(r) - \frac{X_{n\kappa}^P(r)}{r}. \end{aligned} \quad (6)$$

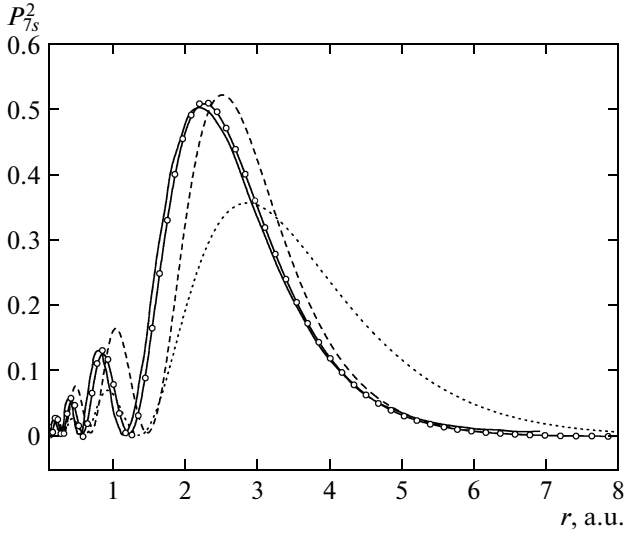


Fig. 1. Calculated electron density $P_{7s}^2(r)$ of the $7s$ orbital in a neutral Rg atom, $Z = 111$. Solid curve — the fully relativistic calculation [25]; dashed curve — the nonrelativistic wave function but the relativistic binding energy, a RICODE result; solid curve with open circles — the relativistic wave function and relativistic binding energy, a RICODE-M result; dotted curve — the fully nonrelativistic calculation

Here, c is a speed of light, $\kappa = (-1)^{l+j+1/2}(j+1/2)$ is the relativistic quantum number, nlj are the principal, orbital, and total angular quantum numbers, $P_{n\kappa}(r)$ and $Q_{n\kappa}(r)$ are the respective large and small components of the Dirac radial wave function, $Y_{n\kappa}(r)/r$ is the Hartree–Coulomb potential, and $X_{n\kappa}^{P(r),Q(r)}/r$ are the inhomogeneous parts of the differential Dirac–Fock equations due to the nonlocal exchange interaction and nondiagonal Lagrange multipliers.

For continuous states, the energies $\varepsilon > 0$ and the radial wave functions are found from Eq. (2) with the same relativistic core potential as for the initial bound state, i. e., the relativistic core potential $U_c(r)$ is represented in the local form for both bound and continuum states. Although the binding energies found in RICODE-M do not completely correspond to the local potential $U_c(r)$, the scaling factor ω corrects this small inconsistency; the calculated ω values are usually close to unity: $\omega \sim 1$.

As an example of the calculated radial wave function, electron densities of the $7s$ orbital in superheavy Rg atoms ($Z = 111$, configuration $6d^9 7s^2$) are presented in Fig. 1. The dotted line represents a fully nonrelativistic calculation, i. e., the one with the nonrelativistic binding energy and the nonrelativistic core

Table 1. Calculated relativistic (ε_{rel}) and nonrelativistic (ε_{nonrel}) binding energies of a neutral Rg atom ($Z = 111$) having the electronic configuration $1s^2 2s^2 \dots 5d^{10} 6s^2 6p^6 5f^{14} 6d^9 7s^2$. ε_{rel} , ε_{nonrel} — the result by the RICODE-M program, ε — relativistic Hartree–Fock calculations [2]

Shell	ε [2], a. u.	ε_{rel} , a. u.	ε_{nonrel} , a. u.
$7s_{1/2}$	0.4276	0.4278	0.2441
$6d_{5/2}$	0.4119	0.4118	0.6477
$6d_{3/2}$	0.5172	0.5171	0.6477
$6p_{3/2}$	2.2765	2.2764	2.3227
$6p_{1/2}$	3.8476	3.8477	2.3227
$6s_{1/2}$	5.3549	5.3564	3.8094
$5f_{7/2}$	3.0226	3.0224	2.7984
$5f_{5/2}$	2.7986	2.7984	2.7984
$5d_{5/2}$	10.1982	10.1979	11.0519
$5d_{3/2}$	11.2795	11.2791	11.0519
$5p_{3/2}$	17.2870	17.2865	16.6413
$5p_{1/2}$	24.6863	24.6874	16.6413
$5s_{1/2}$	28.7578	28.7645	19.7148
...
$1s_{1/2}$	6898.68	6900.22	5481.18

potential $U_c(r)$. The dashed line is a result of the RICODE program with the relativistic binding energy but with a nonrelativistic potential $U_c(r)$, and the line with open circles corresponds to RICODE-M calculations with the relativistic core potential and relativistic binding energy. All three curves are compared with the relativistic coupled-cluster calculations based on the Dirac–Coulomb–Breit Hamiltonian [25]. As can be seen from the figure, the RICODE-M result is very close to the calculations in [25], especially as concerns the main maximum. The relativistic effects increase the maximum value of the $7s$ -electron density by a factor of 1.5 and shift it toward the nucleus. As we see in what follows, this influence on the wave functions changes the electron-loss cross sections by about 30–40% at the maximum.

The influence of the relativistic effects on the binding energies in a neutral Rg atom ($Z = 111$) is illustrated in Table 1, where the nonrelativistic and relativistic results obtained by RICODE-M are compared with relativistic Hartree–Fock calculations [2]. As expected, the effects are very significant (a factor of 1.5) for ns orbitals because only the wave functions

$R_{ns}(r) = P_{ns}(r)/r$ for ns states are nonzero at the origin and are therefore strongly influenced by interaction with the nucleus.

Table 2 shows a comparison of the binding energies ε and mean radii $\langle r \rangle$ for electron states in the uranium atom, calculated by RICODE-M, with relativistic Hartree–Fock calculations [2] and the Hartree–Dirac–Fock approach [4]. A quite good agreement is seen between all the data presented.

2.2. Electron-loss cross sections

In addition to calculating the relativistic core potential, binding energies, and radial wave functions, the RICODE-M program is able to calculate the single-electron loss cross section σ_{EL} for arbitrary many-electron atoms and ions colliding with neutral atoms; this is the main purpose of the program. The computer code is based on the relativistic Born approximation in the momentum-transfer q -representation in which the projectile-ionization matrix element has the form [5]

$$M_{if} = \langle f | (1 - \beta\alpha_z) e^{i\mathbf{q}\cdot\mathbf{r}} | i \rangle, \quad (7)$$

where $\beta = v/c$ is the relativistic factor, α_z is the z -component of the Dirac matrix $\vec{\alpha}$, and $|i\rangle$ and $|f\rangle$ are the complete wave functions of the colliding system in the initial and final states. Using matrix element (7) and separating radial and angular parts in the formula for the electron-loss cross section $\sigma(v)$, we have the following resulting structure of $\sigma_{EL}(v)$ [23]:

$$\sigma_{EL}(v) = \frac{8\pi a_0^2 N_{nl}}{v^2} \int_{q_0}^{\infty} Z_T^2(q) \frac{dq}{q^3} \times \left(|F(q)|^2 + \frac{\beta^2(1 - q_0^2/q^2)}{(1 - \beta^2 q_0^2/q^2)^2} |G(q)|^2 \right), \quad (8)$$

$$v = \beta c, \quad q_0 = (I_{nl} + \varepsilon)/v, \quad (9)$$

where $a_0 \approx 0.5292 \cdot 10^{-8}$ cm is the Bohr radius, v is the ion velocity, n and l are the principal and orbital quantum numbers of the projectile electron shell with the ionization potential I_{nl} and the number of equivalent electrons N_{nl} , ε is the energy of the ejected electron, and Z_T is the effective charge of the target, which in general depends on q and the minimal momentum transfer q_0 .

The term proportional to $|F|^2$ is used for nonrelativistic collisions, and the term proportional to $|G|^2$ takes the relativistic (magnetic) interaction between colliding particles into account.

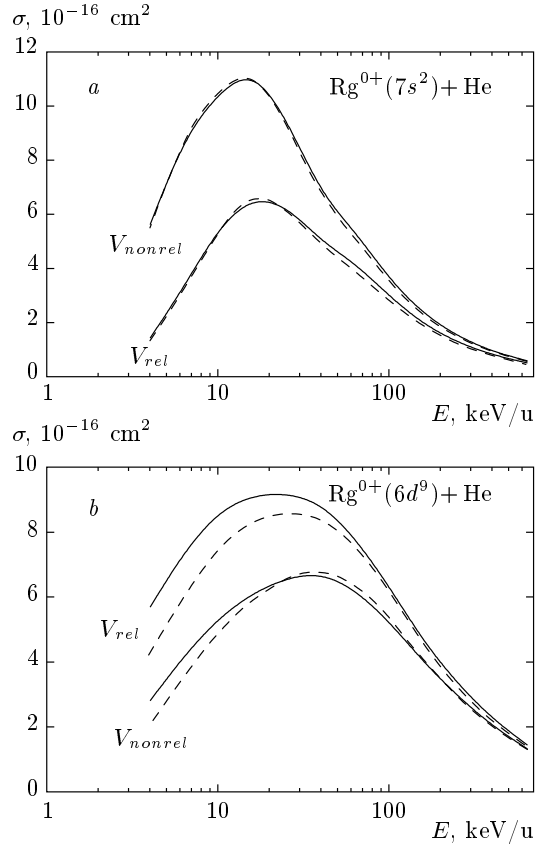


Fig. 2. Electron-loss cross sections of a neutral Rg atom ($Z = 111$) colliding with a He atom followed by the ejection of $7s$ (a) and $6d$ (b) electrons as functions of the collision energy. Dashed curves — calculations with nonrelativistic wave functions for the bound and continuum states, the RICODE program; solid curves — same with relativistic wave functions, the RICODE-M program. V_{rel} and V_{nonrel} indicate the use of relativistic and nonrelativistic interactions in calculation of the electron-loss cross sections

3. NUMERICAL CALCULATIONS OF THE ELECTRON-LOSS CROSS SECTIONS

The results of the numerical calculations of electron-loss cross sections of heavy and superheavy many-electron atoms and ions are presented in Figs. 2–5. The influence of the relativistic effects in the case of collisions between Rg ($Z = 111$) and He atoms is demonstrated in Fig. 2 for the projectile ionization of $7s$ and $6d$ electrons. The difference in cross-section values due to the use of relativistic and nonrelativistic wave functions for the active electron is shown. In both cases, this effect is rather small ($\lesssim 10\%$), although it is somewhat larger for the electron-loss cross section with the ejection of a $6d$ electron. But the influence of the rela-

Table 2. Calculated relativistic binding energies ε and mean radii $\langle r \rangle$ for electronic shells in a neutral U atom ($Z = 92$) having the electronic configuration $1s^2 2s^2 \dots 5d^{10} 6s^2 6p^6 5f^3 6d^1 7s^2$. The data marked “present” represent the result by the RICODE-M program

Shell	ε [2], eV	ε [4], eV	ε present, eV	$\langle r \rangle$ [2], a. u.	$\langle r \rangle$ [4], a. u.	$\langle r \rangle$ present, a. u.
$5f_{7/2}$	8.69	8.71	8.84	1.46	1.46	1.46
$5f_{5/2}$	9.43	9.52	9.56	1.42	1.42	1.42
$6s_{1/2}$	58.16	57.96	58.05	1.50	1.46	1.50
$6p_{3/2}$	26.79	26.67	26.72	1.90	1.90	1.90
$6p_{1/2}$	36.54	36.46	36.37	1.66	1.66	1.67
$6d_{5/2}$	4.99	4.98	5.00	3.29	3.29	3.29
$6d_{3/2}$	5.24	5.25	5.25	3.15	3.15	3.15
$7s_{1/2}$	5.50	5.50	5.50	4.34	4.34	4.35

tivistic interaction between colliding Rg and He atoms is very significant ($\sim 40\text{--}50\%$) for both $7s$ and $6d$ electrons, which is shown in the figure by the difference in the cross sections labeled by V_{rel} and V_{nonrel} . In the case of the ejection of a $7s$ electron, the relativistic interaction leads to a decrease in the cross section, while the electron-loss cross section for a $6d$ electron is increased due to relativistic interaction.

In some cases, a mutual influence of the relativistic effects on the electron-loss cross sections leads to a cancellation effect when the total cross sections calculated with and without the relativistic effects become close to each other, as is seen in Fig. 3, where the electron-loss cross sections for Rg atoms ($Z = 111$) and singly charged Uut atoms ($Z = 113$) colliding with He atoms are shown. We note that in the collision energy range $E < 1$ MeV/u, ejection of $7s$ and $6d$ electrons of Rg atoms (Fig. 3a) makes the leading contribution to the total cross sections (the one summed over all projectile electronic shells).

A similar cancellation effect in the total electron-loss cross sections calculated with the relativistic effects taken into account occurs in collisions of Uut^+ ions with He atoms (Fig. 3b). The rough equality of the total cross sections calculated with and without relativistic effects is also found in theoretical studies of nonradiative electron capture [9], radiative electron capture [26], and radiative recombination [27] processes involving highly charged ions.

Figure 4 shows the influence of relativistic effects on the electron-loss cross sections in collisions of U^{28+} ions with Ar atoms as a function of the ion energy. A contribution of electron ionization from different shells (indicated) and the total cross section of U^{28+} ions by

Ar atoms is shown in Fig. 4a. Solid curves correspond to calculations with relativistic wave functions of the active electron, and dashed curves to those with non-relativistic wave functions; in both cases, the relativistic interaction is used (the second term in Eq. (8)). We can see that in the case of highly charged projectiles, the use of relativistic wave functions leads to a rather small change ($\lesssim 10\%$) of the electron-loss cross sections over the energy range considered. But the influence of the relativistic interaction between colliding particles is extremely large at relativistic energies, which is demonstrated in Fig. 4b by a difference between the solid curve (fully relativistic calculations) and the dashed curve (nonrelativistic calculations).

One of the basic applications of electron-loss cross sections is the determination of beam lifetimes of heavy ions injected into an accelerator. The ion-beam lifetime τ depends on the ion energy, interaction cross sections of the ion beam with the residual atoms and molecules in the accelerator, and the so-called vacuum conditions, i. e., pressure and concentrations of the rest-gas components, which are usually given by a mixture of H_2 , He, O_2 , N_2 , H_2O , CO, CO_2 , CH_4 , and Ar gases. Typical concentrations Y of the basic rest-gas atoms and molecules in accelerators are $Y(H_2) \approx 70\text{--}90\%$, $Y(N_2) \approx 20\text{--}30\%$, and $Y(Ar) \approx 1\text{--}3\%$.

The ion-beam lifetime in an accelerator can be estimated using the formula

$$\tau = \left[\rho \beta c \sum_T Y_T \times \left(\sigma_T^{EC}(q, v, Z_T) + \sigma_T^{EL}(q, v, Z_T) \right) \right]^{-1}, \quad (10)$$

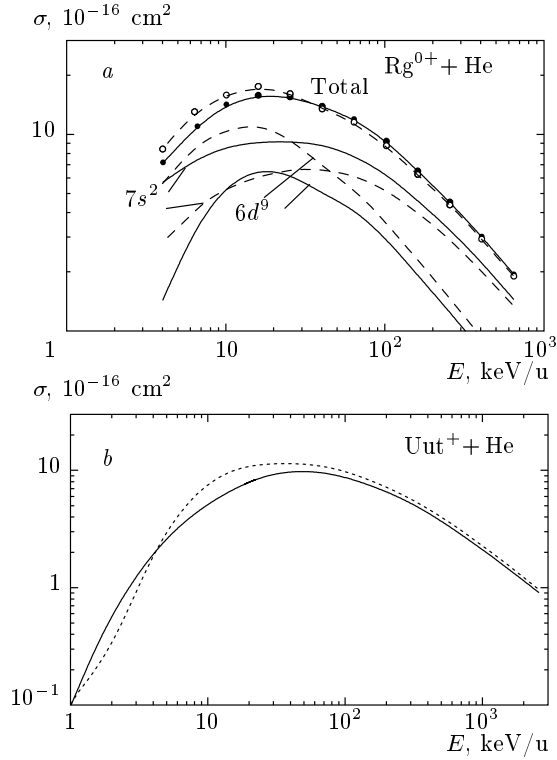


Fig. 3. *a)* Electron-loss cross sections of a neutral Rg atoms ($Z = 111$) colliding with a He atoms, followed by the ejection of $6d$ and $7s$ electrons, and the total cross sections as a function of the collision energy. Dashed curves — the fully nonrelativistic calculations (with nonrelativistic wave functions and interaction); solid curves — the fully relativistic calculations, RICODE-M results. The curves with open circles are the total electron-loss cross sections. *b)* The total electron-loss cross sections of singly charged Uut atoms ($Z = 113$) colliding with He atoms. Dashed curves — the fully nonrelativistic calculations, solid curves — the fully relativistic calculations, RICODE-M results

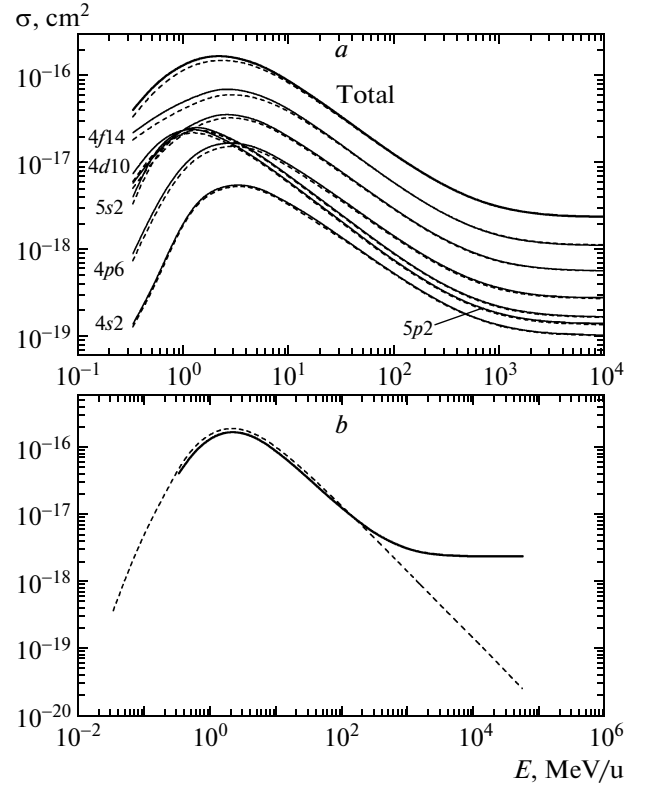


Fig. 4. Electron-loss cross sections of U^{28+} ions ($Z = 92$) in collisions with Ar atoms as functions of the ion energy. *a)* Influence of relativistic wave functions on electron-loss cross sections for the ejection of electrons from different shells of U^{28+} ions. Dashed curves — semirelativistic calculations (with relativistic interaction and nonrelativistic wave functions), solid curves — the fully relativistic calculations, RICODE-M results. *b)* The total electron-loss cross sections calculated in the fully nonrelativistic (dashed curves) and fully relativistic (solid curves) approximations, the RICODE-M results

where ρ denotes the rest-gas density, $\beta = v/c$ is the relativistic factor, q and v are the charge and velocity of the projectile ions, Z_T is the nuclear charge of the rest-gas atoms, and σ^{EC} and σ^{EL} are the total electron-capture and electron-loss cross sections (summed over multi-electron capture and loss processes). The summation over T in (10) is made over all rest-gas components. For molecules, the Bragg additive rule is used: the cross section for a molecule is represented as a sum of those of atoms composing the molecule, e. g., $\sigma(H_2O) = 2\sigma(H) + \sigma(O)$.

In real conditions, the determination the ion-beam lifetime is a much more complicated problem and is not described by Eq. (10) because the rest-gas density and

concentrations Y_T are different in different points of the accelerator volume and are in general time-dependent, and because the rest-gas atoms and molecules can be ionized by the projectile ion beam, leading to a change of the interaction with the projectiles, and so on (see, e. g., [12]). However, the use of Eq. (10) leads to quite reasonable results.

As an example, the experimental lifetime of the U^{73+} -ion beam as a function of the ion energy at specified vacuum conditions is shown in Fig. 5*a* in comparison with the present calculations; the vacuum conditions used in calculations are indicated in the figure. The capture cross sections are calculated using the CAPTURE code described in [28]. As can be seen from

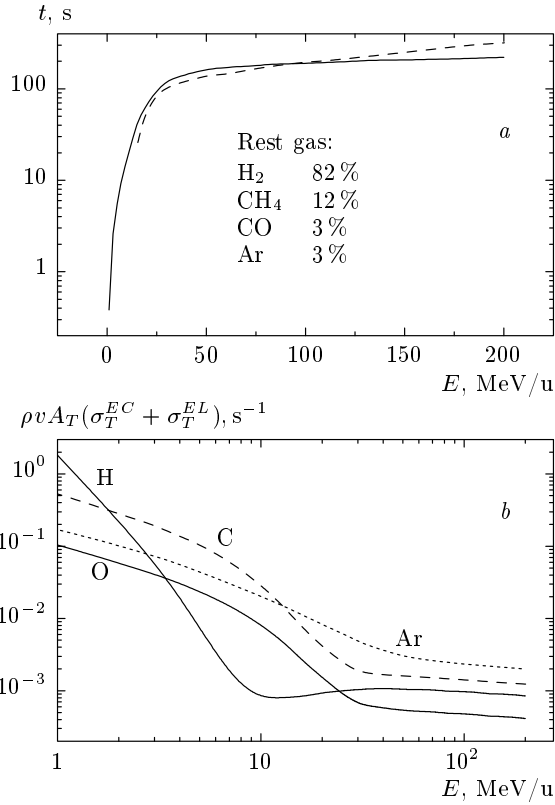


Fig. 5. *a)* Lifetimes of a U^{73+} -ion beam as functions of the ion energy at the rest-gas components shown in the figure. Experiment: dashed lines [29] and [30]; theory: solid lines with the rest-gas density $\rho = 3.4 \times 10^{-10}$ mbar, the RICODE-M result. *b)* Contributions of $\rho v A_T (\sigma_T^{EC} + \sigma_T^{EL})$ values of basic rest-gas atomic components (H, C, O, and Ar) to the sum in (10) as functions of the ion energy, the RICODE-M result. A_T are coefficients accounting for the rest-gas concentrations Y_T , shown in the figure, and the use of Bragg's additive rule: $A_T(\text{H}) = 2.11$, $A_T(\text{C}) = 0.15$, $A_T(\text{O}) = 0.0302$, and $A_T(\text{Ar}) = 0.0325$

the figure, at the given vacuum conditions and energies $E \gtrsim 100$ MeV/u, the lifetime value becomes a constant value, $\tau \sim 300$ s, due to the influence of relativistic effects in the particle interaction: they lead to quasiconstant values of the electron-loss cross sections (see Fig. 4), and, as a consequence, to quasiconstant lifetime values. We note that at energies $E \gtrsim 100$ MeV/u, electron-capture processes do not contribute to the lifetime of the U^{73+} ion beam, but at low energies, on the contrary, electron capture is the main charge-changing mechanism that leads to a decrease in the beam lifetime as the energy decreases.

The calculated contribution of different rest-gas atomic components to the lifetime of U^{73+} -ion beam

is shown in Fig. 5*b*, with each term in the denominator in (10) shown in Fig. 5*a*. The coefficients A_T are the product of the concentrations given in Fig. 5*b* and coefficients following from the Bragg additive rule. As can be seen from the figure, at low energies $E \sim 1\text{--}2$ MeV/u, the main influence on the beam lifetime is due to collisions with light target atoms, H and C, whereas at high energies $E > 100$ MeV/u, the C and Ar atoms are mainly responsible for the ion-beam lifetime in the accelerator.

4. CONCLUSION

We described a newly created RICODE-M computer code, whose purpose is to calculate the electron-loss cross sections of many-electron heavy ions colliding with neutral atoms using relativistic wave functions and relativistic interaction between colliding particles. In the case of heavy and superheavy projectiles (with the atomic number $Z \geq 80$), the use of relativistic wave functions is the most important for low-charged ions; it changes the electron-loss cross section values at energies $E = 20\text{--}50$ keV/u by about 20–30 % around the cross-section maximum compared to the values calculated with nonrelativistic wave functions.

At relativistic energies $E \geq 200$ MeV/u, the relativistic (magnetic) interaction between colliding particles plays a main role and leads to a quasiconstant cross section behavior that limits the lifetimes of highly charged projectile ions in accelerators.

Two of us (IIT and VPS) thank Th. Stöhlker for his hospitality during our stay at GSI/Darmstadt in June 2013.

REFERENCES

1. I. P. Grant, *Adv. Phys.* **19**, 747 (1970).
2. J. P. Desclaux, *Atom. Data Nucl. Data Tabl.* **12**, 311 (1973).
3. R. D. Cowan and D. C. Griffin, *J. Opt. Soc. Amer.* **66**, 1010 (1976).
4. K. G. Dyall and K. Foegri, *Introduction to Relativistic Quantum Chemistry*, Oxford Univ. Press, Oxford (2007).
5. J. Eichler and W. E. Meyerhof, *Relativistic Atomic Collisions*, Acad. Press, New York (1995).
6. J. Eichler and Th. Stöhlker, *Phys. Rep.* **439**, 1 (2007).

7. A. Voitkiv, Phys. Rep. **392**, 191 (2004).
8. A. Voitkiv and J. Ullrich, *Collisions of Structured Atomic Particles*, Springer, Berlin, Heidelberg (2008).
9. I. I. Tupitsyn et al. Phys. Rev. A **82**, 042701 (2010).
10. V. P. Shevelko and H. Tawara, Eds., *Atomic Processes in Basic and Applied Physics*, Springer, Berlin, Heidelberg (2012).
11. I. Yu. Tolstikhina and V. P. Shevelko, Uspekhi Fiz. Nauk **183**, 225 (2013); Phys. Usp. **56**, 213 (2013).
12. C. Omet et al., New J. Phys. **8**, 284 (2006).
13. D. Hoffmann, G. Logan B. Sharkov, et al., Phys. Scripta **123**, 1 (2006).
14. G. Kraft, Progr. Part. Nucl. Phys. **45**, S473 (2000).
15. A. V. Melnikov, A. Alonso, E. Ascasibar et al., Fusion Sci. Technol. **51**, 1 (2007).
16. Yu. Oganessian, Radiochim. Acta **99**, 429 (2011).
17. J. Khuyagbaatar, V. P. Shevelko, A. Borschevsky et al., Phys. Rev. A **88**, 042703 (2013).
18. H.-D. Betz, Rev. Mod. Phys. **44**, 465 (1972).
19. V. P. Shevelko, I. L. Beigman, M. S. Litsarev, H. Tawara, I. Yu. Tolstikhina, and G. Weber, Nucl. Instr. Meth. B **269**, 1455 (2011).
20. V. P. Shevelko, M.-Y. Song, I. Yu. Tolstikhina, H. Tawara, and J.-S. Yoon, Nucl. Instr. Meth. B **278**, 63 (2012).
21. A. D. Voitkiv, B. Najjari, and A. Surzhykov, J. Phys. B: Atom. Mol. Opt. Phys. **41**, 111001 (2008).
22. B. Najjari, A. Surzhykov, and A. B. Voitkiv, Phys. Rev. A **77**, 042714 (2008).
23. G. Baur, I. L. Beigman, V. P. Shevelko et al., Phys. Rev. A **80**, 012713 (2009).
24. V. F. Brattsev, G. B. Deineka, and I. I. Tupitsyn, Izv. Akad. Nauk SSSR **41**, 2655 (1977).
25. E. Eliav, U. Kaldor, P. Schwerdtfeger et al., Phys. Rev. Lett. **73**, 3203 (1994).
26. Th. Stöhlker, C. Kozhuharov, P. H. Mokler et al., Phys. Rev. A **51**, 2098 (1995).
27. W. Shi, S. Böhm, C. Böhme et al., Europ. Phys. J. D **15**, 145 (2001).
28. V. P. Shevelko, O. Rosmej, H. Tawara, and I. Yu. Tolstikhina, J. Phys. B **37**, 201 (2004).
29. A. Krämer, O. Boine-Frankenheim, E. Mustafin et al., Proc. of EPAC, Paris, France (2002), p. 2547.
30. P. Spiller, ICFA Workshop, GSI, Darmstadt (2004).